J. Fluid Mech. (1994), *vol.* 274, *pp.* 69–92

The hydraulic jump in a viscous laminar flow

By F. J. HIGUERA
ETS Ingenieros Aeronáuticos, Pza Cardenal Cisneros, 3, 28040 Madrid, Spain

(Received 19 May 1993 and in revised form 17 February 1994)

The hydraulic jump appearing in the viscous laminar flow of a thin liquid layer over a finite horizontal plate is studied using the boundary-layer approximation for the flow in and around the jump. The position and structure of the jump are determined by numerically solving the resulting problem with a boundary condition at the edge of the plate that expresses the matching of the layer with the shorter region where the liquid turns around and falls under the action of gravity. When the Froude number of the flow ahead of the jump is very large, the jump is much shorter than the horizontal extent of the layer, though still much longer than its depth. An asymptotic description of the inner structure of such a jump is given, building upon the analysis of Bowles & Smith for the short interaction region at the leading end of the jump. This structure consists of a fast moving separated flow in the upper part of the layer that progressively slows down by ingesting new fluid across its lower boundary, until the hydrostatically generated adverse pressure gradient makes it recirculate in the lower part of the layer. The effects of the surface tension and the cross-stream pressure variation owing to the curvature of the streamlines are taken into account in the jump and in the flow approaching the edge of the plate, showing that they can lead to quantitative and also qualitative changes of the jump structure, including a local breakdown of the boundary-layer approximation.

1. Introduction

Steady hydraulic jumps are a common phenomenon in the flow of liquid layers over horizontal solid surfaces. These layers, generated for example by a falling jet striking the solid or by the flow under a sluice gate, evolve smoothly until a certain position, depending on the downstream conditions, at which their depth undergoes a rapid increase. The flow in the layer upstream of the jump may remain laminar for moderately large Reynolds numbers, but its velocity is seldom uniform, except possibly near the beginning of the layer, owing to the action of viscosity. In the case of a falling jet, the Froude number near the impact region can be very large, being of the order of the ratio of the head of the falling liquid to the size of the cross-section of the jet. This is also the order of the square of the maximum possible ratio of liquid depths across the subsequent hydraulic jump, according to the classical theory of Rayleigh, while the observed ratios are much smaller (even for planar flows) when viscous effects play a role upstream of the jump.

An analysis of the motion in the planar or axisymmetric liquid layer upstream of a jump has been carried out by Watson (1964) using the boundary-layer approximation for laminar and (in an approximated form) turbulent flows. Neglecting the effect of the pressure gradient due to the gravity, he found that a self-similar flow sets in after a relatively short adjustment region, which he also analysed by means of an integral method. Applying then the conditions of continuity and of balance of momentum

across the jump, treated as a discontinuity in accordance with the classical theory, Watson obtained a relation between the position of the jump and the depth of the liquid downstream. Finally, noticing that his experimental data for axisymmetric jumps fell systematically somewhat off this theoretical prediction, he went on to explain how the latter can be improved by taking into account the effects of the finite length of the jump in the balance of momentum.

Similar experiments have been performed by Larras (1962), Olsson & Turkdogan (1966), and Nakoryakov, Pokusaev & Troyan (1978), for axisymmetric flows, while the heat transfer characteristics of these flows, of interest for chemical, metallurgical, and microgravity applications, have been investigated by Chaudhury (1964), following the steps of Watson (1964), Rahman, Hankey & Faghri (1991), and experimentally by Ishigai *et al.* (1977). Olsson & Turkdogan measured the liquid depth and found that the surface velocity upstream of the jump decreased with radial distance more slowly than predicted by Watson. Nakoryakov *et al.* showed that negative values of the skin friction occur within the jump, indicating that the boundary layer separates there and a zone of reversed flow exists near the wall.

Craik *et al.* (1981) visualized a substantial region of reversed flow at the bottom of the layer and a rapid forward-moving flow in the upper part, which remains rapid for some distance behind the jump by riding over the slower recirculating fluid with very small friction losses. They measured the liquid depth by a light-absorption technique, pointing out that the surface tension leads to small oscillations of the surface immediately ahead of the main jump, and remarked that the flow within the jump is complex and varies markedly with changing conditions. They also reported an instability of the flow when the radius of the jump is made to decrease, and related the onset of this instability with a critical value of the (local) Reynolds number.

Using flow visualization and laser anemometry, Bouhadef (1978) found that, in some conditions, the jump has a different structure, consisting of a wall jet flowing under a region of lower velocity, and that a continuous transition from supercritical to subcritical flow takes place in the wall jet. He also carried out computations with an integral method and parabolic velocity profiles in the different regions of the flow, claiming good agreement with his experimental results.

The idea that the hydraulic jump in a viscous laminar flow might be a form of boundary-layer separation due to an adverse hydrostatically generated pressure gradient dates back to Tani (1948) and Kurihara (1946), though the conclusions they drew from this idea seem to be incorrect. Gajjar & Smith (1983) analysed the process leading to a hydraulic jump in a uniform velocity layer with a thin viscous sublayer at its bottom in the limit of large Reynolds numbers (based on the depth of the layer). They showed that the jump is the result of a viscous–inviscid interaction taking place in a region that is long compared with the thickness of the liquid layer but short compared with its viscous adjustment length. It is only in a thin viscous sub-sublayer near the wall that the flow reacts to the hydrostatic pressure gradient induced by the displacement of the sub-sublayer itself, and ends up separating from the wall, while the flow in the bulk of the layer is merely displaced upward and does not slow down in the interaction region. Overall, this interaction amounts to a branching of the flow from the upstream unperturbed state, adjusting itself to the downstream conditions. Bowles & Smith (1992) extended this analysis to the realistic situation in which the effect of viscosity extends to the whole incident layer. They studied the important case of large Froude-number flows, in which the interaction region is very short, and found that the effects of surface tension and cross-stream pressure variation due to streamline curvature strongly influence the flow in the interaction region under realistic conditions.

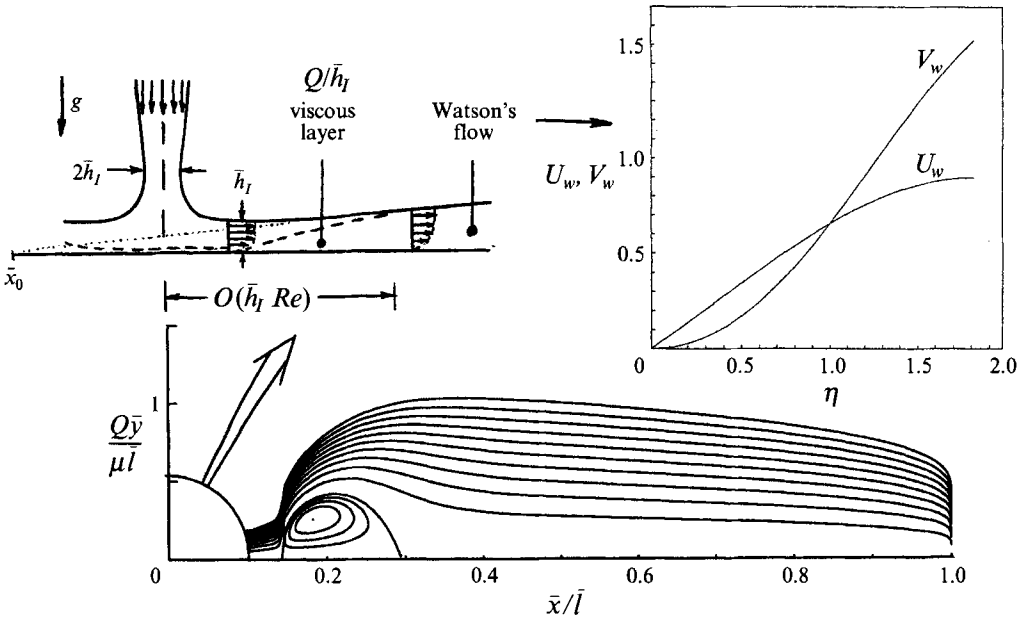

FIGURE 1. Definition sketch, scaled velocities according to Watson's solution, and streamlines of the flow for $S = 9$.

Their results show good agreement with the experimentally determined surface shapes of Craik *et al.* (1981) for the fore part of the jump.

In this paper, the boundary-layer approximation is taken a step forward to describe the flow in the whole of a planar hydraulic jump in the limit of infinite Reynolds numbers. It turns out that the boundary-layer problem is not parabolic for any finite Froude number, and its solution depends on the downstream conditions, which is one of the basic ingredients required for a jump to exist. The other characteristic of a jump, its abruptness in the scale of the overall flow, requires, on the contrary, that upstream information propagation be difficult or inefficient ahead of the jump. In the present viscous flow, this is achieved when the Froude number is very high at the upstream end of the layer. Special attention is therefore paid to the double asymptotic limit of large Reynolds and Froude numbers, looking for the inner structure of the strong jumps that arise in these conditions, which dissipate most of the energy fed into them by the incoming flow. The effects of surface tension and cross-stream pressure variation are also taken into account, and the latter is shown to lead to a qualitative change in the jump structure, involving a local breakdown of the boundary-layer approximation.

The paper is organized as follows. The boundary-layer problem for the planar flow over a finite-length plate is formulated in §2, where some properties of the flow in the asymptotic limits of interest are also discussed. Section 3 is devoted to the numerical solution of the problem, including a brief description of the numerical method used and a discussion of the emerging hydraulic jump and its evolution with increasing Froude numbers. The asymptotic structure of the jump for very large Froude numbers is analysed in §4, which ties in with the description of Bowles & Smith of the flow in the interaction region at the leading end of the jump. Approximate values of the length and depth ratio of the jump, and of the friction with the wall, are obtained. A possible instability is pointed out, suggested by the nature of the flow in the interior of the jump. The effects of surface tension and streamline curvature are discussed in §5, where

another asymptotic structure is proposed for the case in which the second of these effects dominates the flow locally. Lastly, the flow near the edge of the plate, which is an integral part of the problem owing to the upstream-propagating influence mentioned before, is analysed in an Appendix, showing that the subcritical flow approaching the edge speeds up and becomes locally critical.

2. Formulation and orders of magnitude

Consider the laminar two-dimensional flow of a layer of liquid over a horizontal plate of length $2l$ owing to the impact of a vertical planar jet on the centre of the plate (figure 1). Let $2Q$ and $2\bar{h}_I$ be the flux (per unit length) and width of the jet immediately before touching the plate, and $Re = Q/\nu \gg 1$. This $\bar{h}_I$ is also the depth of the liquid layer immediately downstream of the impact region, $O(\bar{h}_I)$, and $Q/\bar{h}_I$ is the uniform horizontal velocity of the flow there. Viscosity will influence the flow in the layer further downstream, in a viscous adjustment region of length $O(\bar{h}_I Re)$, if the length of the plate is comparable to, or much larger than, this value.

In the absence of gravity, the flow beyond the adjustment region tends to a self-similar state (Watson 1964) of the form $\bar{u} = (Q^2/\nu\bar{x})\, U_W(\eta)$, $\bar{v} = (Q/\bar{x})\, V_W(\eta)$, $\bar{h} = H_W \nu\bar{x}/Q$, with $\eta = Q\bar{y}/\nu\bar{x}$. Here $\bar{x}$ is the distance along the plate from the apparent origin of the self-similar flow, $\bar{y}$ is the distance normal to the plate, $\bar{u}$ and $\bar{v}$ are the corresponding components of the velocity, and $\bar{h}$ is the depth of the layer. The functions $U_W(\eta)$ and $V_W(\eta)$ $[= \eta U_W(\eta)]$ are represented in figure 1. Other features of this flow, noted here for further reference, are

$$H_W \simeq 1.8138, \quad U'_W(0) = \int_0^{H_W} U_W^2 \,\mathrm{d}\eta \simeq 0.6930, \quad U_W(H_W) \simeq 0.8964,$$

$$\int_0^{H_W} U_W^3 \,\mathrm{d}\eta \simeq 0.2613.$$

Numerical solution of the relevant boundary-layer equations for the liquid layer with a uniform inlet velocity shows that the self-similar state, which only remembers the value of the flux Q but not $\bar{h}_I$, is already established after an adjustment distance $\bar{x}_1 \simeq 0.3\bar{h}_I\, Re$ downstream of the impact point of the jet, and that the apparent origin is located at a distance $\bar{x}_0 \simeq 0.705\bar{h}_I\, Re$ upstream of this point. Appropriate scales for the depth and velocity of the flow in the layer are therefore $h_c = \nu\bar{l}/Q$ and $u_c = Q^2/\nu\bar{l}$, where $\bar{l} = l + \bar{x}_0$ is the half-length of the plate augmented by the distance to the apparent origin. The distances along the plate are measured from this origin in what follows.

In the limit $Re \to \infty$, in which the liquid layer is infinitely smooth and the vertical accelerations are negligible, gravity leads to a pressure distribution determined by a hydrostatic balance in terms of the local depth. The influence of the gradient of this pressure on the flow is measured by the parameter $S = gh_c/u_c^2 = g\bar{l}^3\nu^3/Q^5$, which is the inverse of a Froude number. Thus gravity does not play any role if $S \ll 1$, and Watson's solution is then applicable down to the edge of the plate, while, on the contrary, this solution becomes invalid on most of the plate if $S \gg 1$, though it can still be valid in a region $\bar{x} = o[Re(Q^2/g)^{\frac{1}{5}}]$ around the centre of the plate when $g\bar{h}_I/(Q/\bar{h}_I)^2 \ll 1$. (Note that this latter condition is commonly satisfied, because $(Q/\bar{h}_I)^2/2g$ is the head of the fluid in the jet, typically large compared with its half-width $\bar{h}_I$. Note also that $g\bar{h}/\bar{u}^2$ is proportional to $S(\bar{x}/\bar{l})^3$ when evaluated with Watson's solution;

this quantity serves as a local inverse Froude number and the previous condition on $\bar{x}$ is obtained by setting it equal to one.) Further discussion of this case and of the case $S = O(1)$ is given later in this section. The analysis of the effects of surface tension and streamline curvature (which is a finite *Re* effect) is deferred until §5.

The flow in the liquid layer obeys the simplified non-dimensional equations (see Bowles & Smith 1992)

$$\frac{\partial u}{\partial x}+\frac{\partial v}{\partial y}=0, \tag{1}$$

$$u\frac{\partial u}{\partial x}+v\frac{\partial u}{\partial y}=-S\frac{\mathrm{d}h}{\mathrm{d}x}+\frac{\partial^2 u}{\partial y^2}, \tag{2}$$

with the boundary conditions

$$u=v=0 \quad \text{at} \quad y=0, \tag{3}$$

$$\frac{\partial u}{\partial y}=0, \quad u\frac{\mathrm{d}h}{\mathrm{d}x}-v=0 \quad \text{at} \quad y=h, \tag{4}$$

$$u=1/h_I, \quad h=h_I \quad \text{at} \quad x=0.705h_I, \tag{5}$$

plus appropriate conditions at the edge of the plate, to be discussed below. The variables x, y, u, v, and h have been made non-dimensional; with the factors $\bar{l}$, h_c, u_c, $u_c h_c/\bar{l}$, and h_c, respectively (in particular, $h_I = \bar{h}_I/h_c$).

A boundary condition is needed at the edge of the plate because the problem is not parabolic when $S > 0$, despite the boundary-layer approximation. This is related to the fact that the pressure gradient $S\,\mathrm{d}h/\mathrm{d}x$ is not given in advance but must be determined as part of the solution, which enables upstream propagation of gravity waves; see the results on wave propagation below. The boundary-layer approximation fails in a region $(1-x) = O(Re^{-1})$ around the edge of the plate because the radius of curvature of the streamlines there is of the order of the thickness of the layer, and the boundary condition sought for should come from matching the boundary layer and this region. It turns out, however, that the matching does not require a detailed analysis of the latter region; it suffices to impose the requirement that the acceleration of the boundary-layer flow must diverge on approaching the edge in anticipation of the much stronger accelerations prevailing in the turn around region, where the action of the gravity is no longer restricted by the presence of the plate. The asymptotic structure that the boundary layer develops for $x \nearrow 1$ (but still $Re\,(1-x) \gg 1$) when subject to this requirement has been analysed elsewhere in connection with other related problems (Daniels 1992; Higuera & Liñán 1993; Higuera 1993), and some of its features are summarized in the first part of the Appendix (equations (A 1)–(A 4) with the subscript e suppressed and $(-x_e)$ replaced by $(1-x)$). Essentially, the horizontal velocity tends to a limiting distribution and the depth tends to a limiting positive value for $x \nearrow 1$, both unknown, which are approached with $\partial(u,h)/\partial x = O[(1-x)^{\delta-1}]$, $\delta \simeq 0.308$. Details on how this boundary condition is implemented in the numerical scheme are given in the next section. It should be noted that an alternative singularity exists for equations (1)–(4) (Brown, Stewartson & Williams 1975; Bowles 1990) in which, up to logarithms, $\mathrm{d}h/\mathrm{d}x = O[(1-x)^{-\frac{3}{5}}]$. The numerical results for this and related problems seem to favour (A 1) over the alternative singularity when the flow near the edge of a plate is at issue.

The solution of (1)–(5) and the boundary condition at the edge determines the distributions of velocity and depth of the layer for given values of S and h_I. That this

problem has regular solutions representing relatively abrupt transitions between different flow regimes (hydraulic jumps) will be shown in the following two sections, and some features of these solutions are discussed in the remainder of this section. While the existence of even sharper transitions, beyond the scope of the boundary-layer approximation, cannot be ruled out (see §5), the results of the following two sections strongly suggest that the length of a stationary jump cannot be arbitrarily small in the absence of turbulence or downstream wave generation.

According to the classical theory, a hydraulic jump is a supercritical-to-subcritical transition of the flow, in the nature of a shock. (Here the flow is said to be subcritical when upstream propagation of small perturbations is possible and supercritical when it is not.) Therefore, an analysis of the propagation of small-amplitude waves in the present viscous flow can provide a guide to situations in which a jump should be expected. The results of this analysis are as follows: (i) the flow near the impact region of the jet, where the viscous boundary layer is still very thin, is supercritical if the local Froude number $S_l^{-1} = (g\bar{h}_l^3/Q^2)^{-1}$ is larger than one and subcritical if it is smaller than one. This is a well-known result. (ii) Upstream propagation is possible in the developing and fully developed flows for any $S > 0$, owing to the presence of a substantial region of low velocity at the bottom of the layer, and becomes impossible only when the local Froude number $S_l^{-1} = (Sx^3)^{-1}$ tends to infinity; see Smith & Brotherton-Ratcliffe (1990).

Guided by these results, let us consider a hydraulic jump sitting in a region of $S_l \ll 1$, which for the flow under scrutiny is the region where Watson's solution would be applicable in the absence of the jump (assuming for the time being that it is in the developed flow). Note that $S_l = Sx_J^3$ immediately ahead of the jump, x_J being the position of its upstream end; obviously a $x_J \ll 1$, and hence a $h_l \ll 1$, is required to have a jump with $S_l \ll 1$. A good deal of information on these jumps is contained in the condition of conservation of the horizontal momentum:

$$\int_0^{h_1} u_1^2 \,\mathrm{d}y + \tfrac{1}{2}Sh_1^2 \sim \int_0^{h_2} u_2^2 \,\mathrm{d}y + \tfrac{1}{2}Sh_2^2, \tag{6}$$

where 1 and 2 denote the sections immediately upstream and downstream of the jump, and the symbol $\sim$, with the meaning that the two sides of (6) are of the same order, is used here instead of the equality because the friction with the plate between the §§1 and 2 has been omitted. As will be seen in §4, the effect of the friction is of the same order as the terms displayed in (6), though these jumps are much shorter than the plate. Since $S_l \ll 1$, the second term on the left-hand side of (6) is much smaller than the first, and this one can be evaluated using Watson's solution, which gives

$$\int_0^{h_1} u_1^2 \,\mathrm{d}y \simeq 0.6930/x_J.$$

Then (6) implies $h_2 = O[(Sx_J)^{-\frac{1}{2}}]$ and, since the mass flux is conserved [$u_2 h_2 = O(1)$],

$$[\tfrac{1}{2}Sh_2^2] \Big/ \int_0^{h_2} u_2^2 \,\mathrm{d}y = O(Sh_2^3) = O(S^{-\frac{1}{2}}x_J^{-\frac{3}{2}}) = O(S_l^{-\frac{1}{2}}) \gg 1,$$

so that the momentum flux is negligible compared with the gravity term at the downstream end of the jump. Had the symbol $\sim$ in (6) been replaced by an equality, these estimations would lead to $h_2 \simeq 1.1773/(Sx_J)^{\frac{1}{2}}$. However, owing to the friction with the plate, the result is $h_2 = \beta/(Sx_J)^{\frac{1}{2}}$, where β is determined by the analysis of the inner

structure of the jump. This analysis, carried out in §4, yields the approximate value $\beta \simeq 1.25$, which is not very different from the factor 1.1773 above, pointing toward a relatively small effect of the friction.

The flow downstream of the jump must be analysed in order to relate the still unknown x_J to S. The previous estimates imply that the convection terms of equation (2) are negligible in this region, and then the balance of viscous and pressure forces, i.e. $S\,\mathrm{d}h/\mathrm{d}x = \partial^2 u/\partial y^2$, with $u(0) = (\partial u/\partial y)(h) = 0$, gives $u = -(\frac{1}{2}S)(\mathrm{d}h/\mathrm{d}x)\,y(2h-y)$, whereas the condition $1 = \int_0^h u\,\mathrm{d}y = -(\frac{1}{3}S)\,h^3(\mathrm{d}h/\mathrm{d}x)$ implies $h^4(x) - h^4(1) = 12(1-x)/S$. Moreover, it is shown in the Appendix that the effects of inertia reappear at a short distance from the edge of the plate, where the flow speeds up and becomes locally critical. This is accomplished through a pronounced decrease of the depth of the liquid, so that the appropriate boundary condition for the viscous-dominated flow, required for matching with the aforesaid region, is $h(1) = 0$, leading to $h(x) = [(12/S)(1-x)]^{\frac{1}{4}}$ downstream of the jump, and to $h_2 \simeq (12/S)^{\frac{1}{4}}$ (because $x_J \ll 1$). Therefore, compatibility with the h_2 obtained in the previous paragraph requires

$$x_J = \frac{\beta^2}{12^{\frac{1}{2}} S^{\frac{1}{2}}}. \tag{7}$$

Other quantities of interest are

$$h_1 \simeq \frac{0.5236\beta^2}{S^{\frac{1}{2}}}, \quad \frac{h_2}{h_1} \simeq 3.5546 \frac{S^{\frac{1}{4}}}{\beta^2}. \tag{8}$$

Note that (7) implies $S \gg 1$ and $S_l = O(S^{-\frac{1}{2}})$. Then, from (8), $h_2/h_1 \gg 1$ for these jumps, which are therefore very strong according to the classical classification.

The upstream displacement of the jump with increasing S comes to an end when x_J in (7) becomes comparable to the adjustment length of the flow (of order h_I in non-dimensional variables), which happens for $S = O(h_I^{-2})$. Thus a strong jump exists in the region of fully developed flow for $1 \ll S \ll h_I^{-2}$. As will be seen in the next section, no hydraulic jump exists at all for values of S much larger than h_I^{-2}, while, at the other extreme, the strength of the jump decreases when S decreases, becoming a smooth elevation of the surface, of length comparable to that of the plate, when $S = O(1)$.

The other supercritical flow condition, pointed out by the result (i) of the wave propagation analysis, is covered by the work of Gajjar & Smith (1983), who described the leading part of a jump in an almost uniform flow like the one near the impact region of the jet for $S_l^{-1} = (g\bar{h}_I^3/Q^2)^{-1} = O(1) > 1$. Such a jump can be realized in the present finite plate configuration for $h_I = O(1)$ (corresponding to plate lengths of the order of the adjustment length of the flow), in which case $S = O(1)$ and the size of the jump turns out to be comparable to the length of the plate. This jump is pushed into the region of non-uniform flow when $h_I \ll 1$ keeping $S = O(1)$, because the foregoing estimates require that $x_J = O(1)$. This provides a link with the smooth surface elevations mentioned before.

A few comments about the choice of the present geometrical configuration seem appropriate to close this section. As shown by Bohr, Dimon & Putkaradze (1993), no stationary solution exists beyond the jump for an infinitely long horizontal plate when the friction with the plate is taken into account. Obviously, the idea of a constant liquid depth downstream of the jump makes no sense here, and a complex influence of the actual conditions away from the jump is at work. While many details of the far field may be irrelevant to the flow ahead and around the jump (specially in the limit of very strong jumps analysed in §4), they lead to difficult problems when a mathematically

closed formulation is sought. On the contrary, a finite-size plate provides a clean cut for the flow in the layer, because, as mentioned before, this flow becomes critical on approaching the edge, and therefore independent of the conditions further downstream.

3. Numerical solutions

3.1. *Numerical method*

For the numerical treatment, the second condition (4) is replaced by the equivalent condition of conservation of the flux

$$q \equiv \int_0^h u \, dy = 1, \tag{9}$$

obtained by integrating the continuity equation (1) across the layer and using (5). The variable $z = y/h(x)$ is used instead of y to reduce the computational domain to a square.

The singularity (A 1) of the boundary-layer solution at the edge of the plate is handled numerically by introducing the strained variable

$$\xi = 1-(1-x)^{\varphi}, \quad \text{with } 0 < \varphi < 1, \tag{10}$$

instead of x, so that, for example, $\partial u/\partial\xi = (1-x)^{1-\varphi}(\partial u/\partial x)/\varphi = O[(1-x)^{\delta-\varphi}]$ for $(1-x) \ll 1$ (see (A 1)), which remains finite if $\varphi < \delta$. Using the strained variable (10) and an extrapolation boundary condition amounts to setting an upper limit to the worse (algebraic) singularity that the solution can develop at the edge, but it is the solution itself which selects the strength of the singularity in the range $\varphi < \delta < 1$, and a logarithmic plot of $\partial u/\partial x$ versus $(1-x)$ shows that the selected δ is the one predicted by the analysis of the Appendix (see Higuera (1993) for further details and a parametric study for different values of φ). An appropriate treatment of the viscous sublayer where (A 4) holds would also require a strained z-coordinate, but this sophistication was not included here, while still keeping good resolution until very close to the edge, by the simpler procedure of using a fine grid near the bottom of the layer.

The resulting equations are discretized using upwind finite differences for the convective terms and centred differences for the viscous and pressure gradient terms. A pseudotransient iteration is used, which amounts to adding a term proportional to $\partial u/\partial t$ to the left-hand side of (2), but not to the condition of conservation of the flux (9) (which should be replaced by $\partial h/\partial t + \partial q/\partial x = 0$ to describe a real transient). The viscous and pressure gradient terms (along with (9)) are treated implicitly, and the convective terms explicitly.

The independence of the results of the numerical parameters was checked by changing the number and distribution of grid points and the value of φ. Typically grids of 240×60 or 350×80 points and $\varphi = \frac{1}{4}$ were used to obtain the results that follow.

3.2. *Results and discussion*

Consider first the limit $h_I \to 0$. In this limit the adjustment length of the flow is negligible compared to the length of the plate and Watson's solution is attained very rapidly. Hence, the inlet conditions (5) can be replaced by their limiting form

$$u = \frac{1}{x} U_W(H_W z), \quad h = H_W x \quad \text{for } x \to 0, \tag{11}$$

which are applied by rewriting the problem in terms of xu and xv. When S is small, the

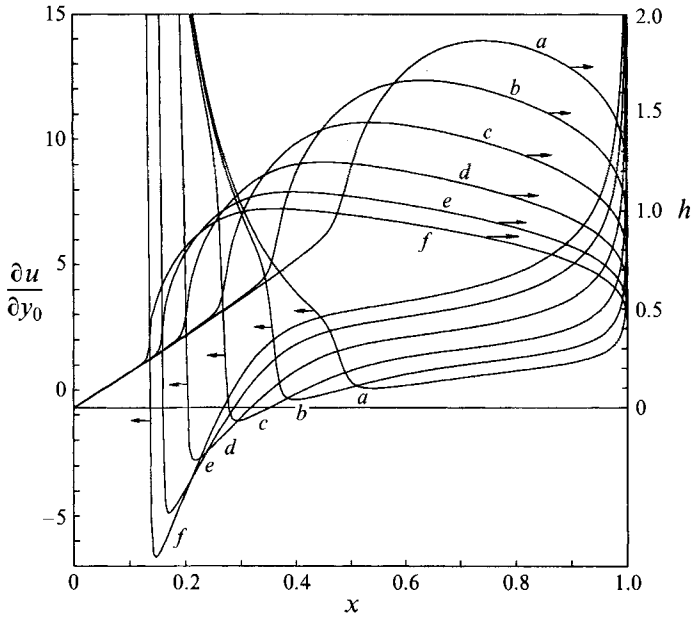

FIGURE 2. Skin friction and liquid depth for several values of S with the boundary conditions (11). *a*, $S = 0.5$; *b*, $S = 1$; *c*, $S = 2$; *d*, $S = 4$; *e*, $S = 7$; *f*, $S = 10$.

flow is seen to remain supercritical over the whole layer, and the condition at $x = 1$ has very little effect. As S increases, the depth of the layer near the edge first rises faster than linearly and then decreases under the action of the condition at the edge. An incipient hydraulic jump begins to form and moves steadily upstream and develops a recirculation bubble at the bottom as S is further increased, until a form of fully developed jump comes into existence when S is still $O(1)$. The size of this jump, however, is comparable to that of the plate, so that it can hardly be considered an abrupt transition. This structure evolves without apparent qualitative changes, moving upstream and decreasing in size as S increases. The streamlines in figure 1 are for $S = 9$, and figure 2 shows the distributions of wall shear stress and depth for several S. As can be seen, the depth upstream of the jump increases linearly with the distance from the origin, reflecting very little influence of the gravity in this region. Then, the depth rises very rapidly, even at these moderate values of S, and the recirculation bubble takes a quasi-parabolic shape near its leading tip (figure 1), which is in qualitative agreement with the predictions of Bowles & Smith (1992). The rear tip of the bubble is only slightly upstream of the point of maximum depth, and the distance between these points decreases with increasing S (figure 2). That the recirculation bubble be always in the region of increasing depth is a necessary condition for its equilibrium, because the resultant pressure force on the bubble must be directed toward the left in figure 1 to balance the shear forces exerted by the wall and by the fluid flowing above the bubble, which are directed toward the right. Figure 3 gives the position of the jump, defined by the leading tip of the recirculation bubble, and the ratio of the maximum depth to the depth at the separation section for several values of S. The agreement of x_J with the asymptotic result (7) is good even for moderate values of S.

The fluxes of momentum and energy,

$$\phi_M = \int_0^h u^2 \,\mathrm{d}y + \tfrac{1}{2}Sh^2, \quad \phi_E = \int_0^h \tfrac{1}{2}u^3 \,\mathrm{d}y + Sh,$$

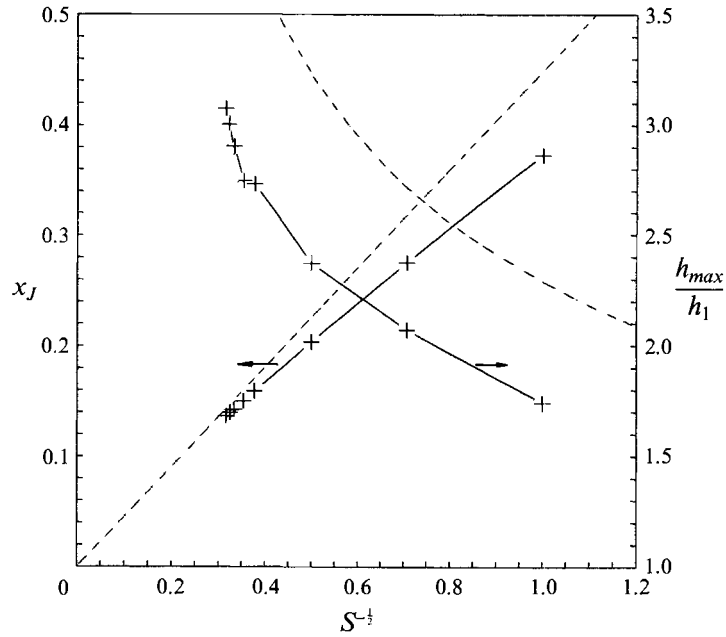

FIGURE 3. Leading end of the jump and ratio of depths for several values of S. The dashed lines represent the asymptotic results (7) and (8) for $S \gg 1$.

respectively, obey $$\frac{d\phi_M}{dx} = -\frac{\partial u}{\partial y}\bigg|_{y=0}, \quad \frac{d\phi_E}{dx} = -\int_0^h \left(\frac{\partial u}{\partial y}\right)^2 dy. \tag{12}$$

Upstream of the jump, both quantities are almost independent of S and very close to $\phi_{M_W} = 0.6930/x$ and $\phi_{E_W} = 0.2613/x^2$, which correspond to Watson's solution. A large fraction of the total dissipation actually occurs in this region, and it is by this means that the very large depth predicted by the inviscid theory for the layer downstream of the jump is avoided. Then ϕ_E keeps on decreasing inside the jump, at a rate that can be very high for large values of S, and the ratio of energy fluxes across the jump decreases in qualitative agreement with the asymptotic result $\phi_{E_2}/\phi_{E_1} \simeq 1.1874\beta^4/S^{\frac{1}{4}} \ll 1$ for $S \gg 1$ (obtained from the analysis of the previous section). This means that most of the energy entering the jump (mostly kinetic energy) is dissipated in its interior, a feature shared by any strong jump, either laminar or turbulent, and implying that such jumps cannot be very short, and that their existence depends on whether a sufficiently dissipative inner structure actually exists. This issue will be taken up in the following section. To see how the dissipation is brought about, note that the front of the bubble is close to the surface of the liquid, leaving only a narrow passage which becomes narrower as S increases (see figure 1). Thus the flow is forced to maintain a high velocity in this region, and the dissipation rate is correspondingly large. The quantity $(\frac{1}{2}u^2 + Sh)$, which would be constant on each streamline in the absence of viscosity, increases along the streamlines entering the jump very close to the wall, with small velocity, and decreases along all the other streamlines, and most of this decrease occurs in the narrow passage above the bubble.

Further computations were carried out using the inlet condition (5) to study the influence of the adjustment region of the flow when $h_I > 0$. The resulting position of the jump is given in figure 4 for different values of h_I. The value of x_J decreases more

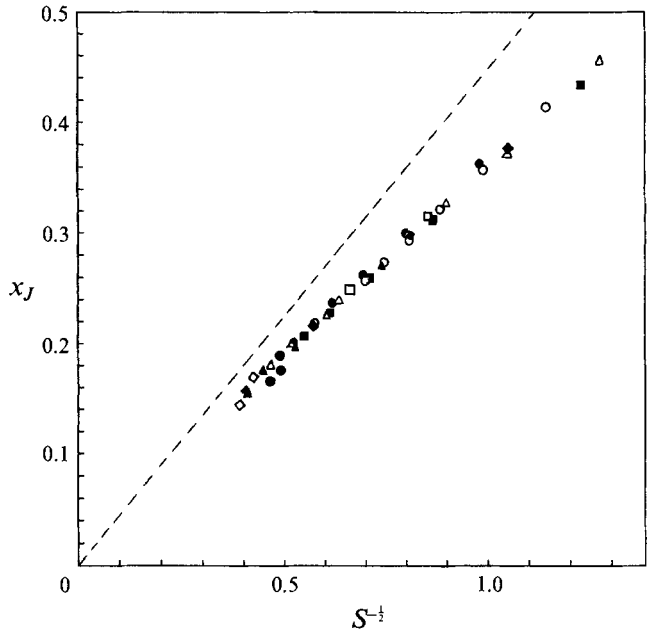

FIGURE 4. Leading end of the jump as a function of S with the inlet conditions (5) and several values of h_I. ▲, $h_I = 0.0934$; △, $h_I = 0.1030$; ■, $h_I = 0.1149$; □, $h_I = 0.1298$; ◆, $h_I = 0.1491$; ◇, $h_I = 0.1753$; ●, $h_I = 0.2125$; ○, $h_I = 0.2699$. The dashed line represents the result (7).

rapidly with increasing S when the jump is in the adjustment region ($x \leqslant 1.005h_I$) than when it is in the region of developed flow, and a small increase of S suffices to make the jump crash onto the inlet once $x_J \simeq 1.005h_I$. This gives rise to another flow regime in which the jet gets submerged before touching the plate; such solutions, and the possible existence of a range of multiplicity, will not be discussed here. The last few points at the left end of some of the sequences in figure 4, which are below the average, represent jumps sitting in the adjustment region. The small separations of the points in the central part of the figure from a common curve are a measure of the numerical errors, since all the data for a given h_I were computed with the same number and distribution of grid points, which were changed from one h_I to another, using finer grids for smaller values of h_I.

4. Structure of the jump for very large values of S

The question of whether an inner structure of the jump exists providing the high dissipation rate required for very large local Froude numbers will be addressed here. For the purposes of this section, the variables $\tilde{x} = x/x_J - 1$, $\tilde{y} = y/x_J$, $\tilde{h} = h/x_J$, $\tilde{u} = x_J u$, and $\tilde{v} = x_J v$ will be used. The boundary-layer problem (1)–(4) conserves the same form when written in terms of these new variables, with S replaced by $S_l = Sx_J^3$. This is a small parameter, $O(S^{-\frac{1}{2}})$, when x_J is taken from (7).

Bowles & Smith (1992) (see also Gajjar & Smith 1983) described the leading end of the jump for $S_l \ll 1$ (region I of figure 5) as a viscous–inviscid interaction region of length $O(S_l^3)$ where the gravity-induced pressure (as well as the surface tension and the cross-stream pressure variations due to the curvature of the streamlines, to be discussed in the following section) influence the flow in a viscous sublayer of thickness $O(S_l)$. Numerical solution of the resulting free interaction problem led Bowles & Smith to the

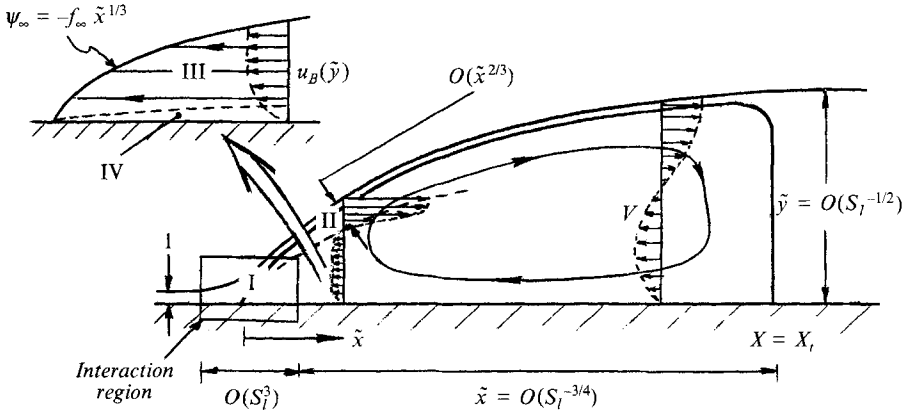

FIGURE 5. Sketch of the asymptotic structure of the jump for $S \to \infty$.

conclusions that the flow separates from the plate leaving an effectively inviscid recirculation region of thickness $O[S_l(\tilde{x}/S_l^3)^m]$ for $\tilde{x}/S_l^3 \gg 1$, with $m = \frac{2}{3}(\sqrt{7}-2)$ determined from the analysis of a viscous sublayer that appears at the bottom of the recirculating flow, and that viscous effects are confined to this sublayer and to a shear layer of thickness $O[(\tilde{x}/S_l^3)^{\frac{1}{3}}]$ between the recirculation region and the separated layer. Neither the forward moving flow nor the flow in the bulk of the recirculation region are affected by the pressure gradient, which is only felt by the weaker flow in the viscous sublayer.

The shear layer at the bottom of the separated flow grows until, for $\tilde{x} = O(1)$, the effect of the viscosity extends to the whole of this flow and the scalings of Gajjar & Smith need modification. Since the influence of the pressure gradient is still negligible in this region (because $S_l \ll 1$), the downstream evolution of the flow coincides with that of (half) a two-dimensional jet issuing from a slit with an initial velocity distribution given by Watson's solution and its mirror image across the free surface. In particular, the mass flux of this jet, $2\psi_\infty(\tilde{x})$ say, can be easily computed by solving a standard parabolic problem. For $\tilde{x} \gg 1$, the flow in the jet takes on the self-similar Bickley's form (see, e.g. Batchelor 1970)

$$\tilde{\psi} = \tilde{x}^{\frac{1}{3}} f(\zeta), \quad \text{with } \zeta = \frac{\tilde{y}-\tilde{h}}{\tilde{x}^{\frac{2}{3}}}, \tag{13}$$

where $3f''' + f'^2 + ff'' = 0, f(0) = f''(0) = f'(-\infty) = 0$, and $\int_{-\infty}^{0} f'^2 \, d\zeta = \Phi_{M_W} \approx 0.6930$, whose solution is $f = f_\infty \tanh(f_\infty \zeta/6)$, with $f_\infty = f(-\infty) = -3^{\frac{2}{3}}\Phi_{M_W} \approx -1.8407$. Here Φ_{M_W} is the momentum flux of Watson's flow immediately ahead of the jump, which is conserved through the interaction region and beyond, as far as the effect of the pressure gradient remains negligible. This effect comes finally into play when $\tilde{u}^2 = (\partial\tilde{\psi}/\partial\tilde{y})^2 = O(\tilde{x}^{-\frac{2}{3}})$ becomes of the order of $S_l\tilde{h}$. By then the thickness of the jet is already comparable to that of the whole layer (see below), and therefore $\tilde{h} = O(\tilde{x}^{\frac{2}{3}})$, which implies $\tilde{x} = O(S_l^{-\frac{3}{4}})$ and $\tilde{h} = O(S_l^{-\frac{1}{2}})$.

Before discussing the flow in this latter region, which is the bulk of the bubble, let us consider the recirculating flow beneath the jet for $\tilde{x} \ll S_l^{-\frac{3}{4}}$. When $\tilde{x}$ is sufficiently large, but still much smaller than $S_l^{-\frac{3}{4}}$, the structure of this flow bears some resemblance to that of Gajjar & Smith (1983) in that it is made of an effectively inviscid region III and a thinner viscous sublayer IV (figure 5), and that, calling $\tilde{y} = \tilde{y}_B \equiv \alpha\tilde{x}^n$ and $\tilde{u} = u_B(\tilde{y}) < 0$ the thickness of the bubble and the velocity of the backflow in III, the local pressure gradient is too weak to affect the flow in III (because this flow comes from a

region to the right where the depth is much larger than in the region of concern, and the Bernoulli constant on its streamlines is therefore much larger than $S_l \tilde{y}_B$). Hence the velocity is constant on each streamline and the balance between the entrainment of the jet and the recirculating flow (i.e. $(\mathrm{d}\psi_\infty/\mathrm{d}\tilde{x})\,\mathrm{d}\tilde{x} = -u_B(\mathrm{d}\tilde{y}_B/\mathrm{d}\tilde{x})\,\mathrm{d}\tilde{x}$, with $\psi_\infty = (-f_\infty)\,\tilde{x}^{\frac{1}{3}}$ and $\tilde{x} = (\tilde{y}/\alpha)^{1/n}$; see figure 5), gives

$$-u_B(\tilde{y}) = \frac{(-f_\infty)}{3n}\frac{\tilde{y}^{(1-3n)/3n}}{\alpha^{1/3n}}. \tag{14}$$

Next, call $\tilde{y}_v(\tilde{x})$ the thickness of the viscous sublayer IV. The velocity in this region is $\tilde{u} = \tilde{u}_v = O[u_B(\tilde{y}_v)]$, to match III, and the balance of convection, viscous force, and pressure gradient, which is required to have a $\tilde{y}_v(\tilde{x})$ decreasing in the direction of the flow, gives the relations $\tilde{u}_v^2/\tilde{x} \sim S_l \tilde{y}_B/\tilde{x} \sim \tilde{u}_v/\tilde{y}_v^2$. Here the approximation $\tilde{h} \approx \tilde{y}_B$ has been used because the jet is still much narrower than the bubble. These relations, along with (14), yield

$$\left.\begin{aligned} &\tilde{y}_v = O[\alpha^{1/1+3n}\,\tilde{x}^{3n/1+3n}], \quad \alpha = \frac{\bar{\alpha}}{S_l^{(2-3n)/4}}, \quad \text{with } \bar{\alpha} = O(1) \text{ unknown,} \\ &n = \tfrac{1}{6}((73)^{\frac{1}{2}} - 7) \simeq 0.2573. \end{aligned}\right\} \tag{15}$$

As can be seen, $O(\tilde{y}_B) = O(\tilde{y}_v) = O(\tilde{x}^{\frac{2}{5}})$ and $O(\tilde{u}_B) = O(\tilde{u}_v) = O(\tilde{x}^{-\frac{1}{3}})$ for $\tilde{x} = O(S_l^{-\frac{3}{4}})$, meaning that the three layers II–III–IV merge to form the bulk of the bubble (region V), as was suggested before.

The results (15) hold for $1 \ll \tilde{x} \ll S_l^{-\frac{3}{4}}$. Let us consider now the recirculation region for $\tilde{x} = O(1)$, where $\psi_\infty(\tilde{x})$ changes from $O(\tilde{x}^{\frac{2}{3}})$ for $\tilde{x} \ll 1$ to $O(\tilde{x}^{\frac{1}{3}})$ for $\tilde{x} \gg 1$. The velocity of the flow entering this region from the right is still given by (14) for $\tilde{y}_v \ll \tilde{y} < \alpha\tilde{x}^n$ (because this fluid left the viscous sublayer when $\tilde{x}$ was large) and the flow keeps on moving horizontally until it is ingested by the shear layer. The height of this shear layer above the plate results from a balance similar to the one sketched in the excerpt of figure 5 for region III, which yields $\tilde{y}_B(\tilde{x}) = \alpha[\psi_\infty(\tilde{x})/(-f_\infty)]^{3n}$. This result applies while $\tilde{y}_B \gg \tilde{y}_v(\tilde{x} = 1)$, i.e. for $S_l^{3(2-3n)/8} \ll \tilde{x} \ll 1$. The solution for still smaller values of $\tilde{x}$ depends on the evolution of the viscous sublayer in the region $\tilde{x} = O(1)$, which will not be discussed here. The asymptotic structure of Gajjar & Smith (1983) for the recirculation region should be retrieved from this solution for sufficiently small values of $\tilde{x}$.

Let us return now to region V. Appropriate variables for this region are $X = S_l^{\frac{3}{4}}\tilde{x}$, $Y = S_l^{\frac{1}{2}}\tilde{y}$, $U = \tilde{u}/S_l^{\frac{1}{4}}$, $V = \tilde{v}/S_l^{\frac{1}{2}}$, and $H = S_l^{\frac{1}{2}}\tilde{h}$. To leading order in an expansion in powers of $S_l^{\frac{1}{4}}$, the equations rewritten in these variables coincide with (1)–(4), with S set equal to one; the upstream boundary conditions, required to match the previous stage, are

$$H = \bar{\alpha}X^n, \quad U = \begin{cases} \dfrac{f'(\zeta)}{X^{\frac{1}{3}}} & \text{if } \zeta = \dfrac{Y-H}{X^{\frac{2}{3}}} = O(1) \\ \dfrac{f_\infty}{3n\bar{\alpha}^{1/3n}}\,Y^{(1-3n)/3n} & \text{if } H - Y = O(X^n) \end{cases} \quad \text{for } X \to 0; \tag{16}$$

and (9) becomes $\int_0^H U\,\mathrm{d}Y = 0$. This last condition expresses the fact that practically all the flux ingested by the jet on top of the bubble, $O(S_l^{-\frac{1}{2}}) \gg 1$ in the previous tilde variables, must recirculate in its rear part.

The resulting problem was solved numerically using the method described in the previous section (with some minor modifications resulting from replacing (9) by the

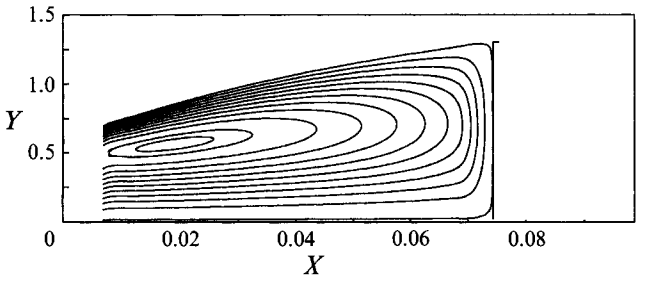

FIGURE 6. Flow in the recirculation region in the limit $S \to \infty$.

condition of zero flux). A condition of extrapolation was applied at a downstream section located far enough to guarantee the independence of the results of this condition. (This can be easily achieved, since the velocity rapidly goes to zero downstream by virtue of the condition of zero flux.) At the inlet, at a value of X ranging from 0.01 to 0.005, the condition (16) for H (with $\bar{\alpha}$ unknown) was replaced by the relation $\mathrm{d}H/\mathrm{d}X = nH/X$, obtained by differentiating (16), which lets H adjust itself to its correct value. The condition (16) for the velocity was realized approximately by imposing an inlet velocity equal to that of the incoming jet on the upper portion of the layer (down to a value of ζ corresponding to 80–90 % of the whole flux) and letting the fluid flow out on the rest of this section. This procedure represents a truncation of the self-similar jet velocity profile, and an artificial adjustment region is thereby induced, so that the point $X = 0$ in figure 6, which shows the result of the computations, need not coincide with the origin of the bubble. From the numerical solution, the value of $\bar{\alpha}$ was found to be about 3, though no great accuracy is claimed for this or the following numerical results.

At this leading order, the velocity of the flow is zero and the depth of the layer takes a constant value $H_0 \simeq 1.25$ beyond a point X_t at a finite distance from the beginning of the bubble (see figure 5). Coming back to the original variables, this H_0 can be seen to coincide with the factor β introduced in §2. Knowledge of β, which is only approximate from these computations, completely determines the position and strength of the jump for a given $S \gg 1$, via (7) and (8).

The structure of the solution for $0 < (X_t - X) \ll 1$ deserves further analysis. Since the velocity tends to zero at $X = X_t$, a local expansion of the form $U = (X_t - X)^j U_0(Y) + \ldots$ seems appropriate. Values of j different from one can be ruled out by the following reasonings. If $j > 1$, the viscous force would dominate over the convection term in the momentum equation and the local expansion of the depth would be of the form $H - H_0 = -(X_t - X)^{j+1} A_0/(j+1) + \ldots$. However, (2)–(4) give then a parabolic distribution for U_0 (as in §2), which cannot satisfy the condition of zero flux

$$\int_0^{H_0} U_0 \, \mathrm{d}Y = 0.$$

If, on the contrary $j < 1$, the viscous term would be negligible in the bulk of the layer and the expansion of the liquid depth would be of the form $H - H_0 = -(X_t - X)^{2j} A_0/2j + \ldots$. Now (1)–(4) have a solution (proportional to (19) below) satisfying the condition of zero flux, but with $U_0(0) = -U_0(H_0) \neq 0$, so that a viscous sublayer of thickness $(X_t - X)^{(1-j)/2}$ is required to satisfy the no-slip condition. However, the solution in this sublayer would be one of the Falkner–Skan family,

with a singularity at $X = X_t$ which probably cannot be removed by a more local analysis. One is therefore left with $j = 1$. In this case the viscous and convection terms in (2) are of the same order, but it turns out that the resulting problem for $(U_0(Y), A_0)$ has no solution (as could perhaps have been expected, because the flow in the upper part of the layer resembles a boundary layer directed toward a stagnation point). These results suggest that logarithmic terms might exist in the expansion: $U = (X_t - X)\{[-\ln(X_t - X)]^k U_0(Y) + \ldots\}$, with $k > 0$, in such a way that, formally, the effect of the viscosity is still confined to a sublayer of thickness $[-\ln(X_t - X)]^{k/2}$ (hence with only a mild singularity at $X = X_t$) while the flow in the upper part of the layer can recirculate as for $j < 1$. Matching of these two regions is possible for $k = 2$ (see the comments at the end of the paragraph following (22)) and, advancing this result, the solution in the outer region ($Y = O(1)$) is sought in the form

$$\left.\begin{aligned} U &= (X_t - X)\{[-\ln(X_t - X)]^2 U_0(Y) + [-\ln(X_t - X)] U_1(Y) + \ldots\}, \\ V &= [-\ln(X_t - X)]^2 V_0(Y) + [-\ln(X_t - X)] V_1(Y) + \ldots, \\ H &= H_0 - \tfrac{1}{2}(X_t - X)^2\{[-\ln(X_t - X)]^4 A_0 + [-\ln(X_t - X)]^3 A_1 + \ldots\}. \end{aligned}\right\} \tag{17}$$

Inserting these expansions into the equations of motion and boundary conditions, and separating like powers of $-\ln(X_t - X)$, we obtain, to leading order,

$$U_0 - V_0' = 0, \quad -U_0^2 + V_0 U_0' + A_0 = 0, \quad V_0(0) = U_0'(H_0) = V_0(H_0) = 0, \tag{18}$$

where the primes denote Y-derivatives. The solution of (18) is

$$U_0 = -\frac{\pi V_m}{H_0}\cos\frac{\pi Y}{H_0}, \quad V_0 = -V_m \sin\frac{\pi Y}{H_0}, \quad A_0 = \frac{\pi^2 V_m^2}{H_0^2}, \tag{19}$$

with V_m arbitrary. Since $U_0(0) \neq 0$, a boundary layer is required, as was advanced before, where $\bar{Y} = [-\ln(X_t - X)]\, Y = O(1)$ and the solution is of the form

$$\left.\begin{aligned} U &= (X_t - X)\{[-\ln(X_t - X)]^2 \bar{U}_0(\bar{Y}) + [-\ln(X_t - X)] \bar{U}_1(\bar{Y}) + \ldots\}, \\ V &= [-\ln(X_t - X)] \bar{V}_0(\bar{Y}) + \bar{V}_1(\bar{Y}) + \ldots. \end{aligned}\right\} \tag{20}$$

Then, to leading order, equations (1)–(3) and the condition of matching with (19) give (primes denoting now $\bar{Y}$-derivatives),

$$\bar{U}_0 - \bar{V}_0' = 0, \quad -\bar{U}_0^2 + \bar{V}_0 \bar{U}_0' + A_0 = \bar{U}_0'', \quad \bar{U}_0(0) = \bar{V}_0(0) = 0, \quad \bar{U}_0(\infty) = -\frac{\pi V_m}{H_0}. \tag{21}$$

From the numerical solution of this problem, $\bar{V}_0 \to -(\pi V_m/H_0)\,\bar{Y} + \mathscr{A}(\pi V_m/H_0)^{\frac{1}{2}}$ for $\bar{Y} \to \infty$, with $\mathscr{A} \simeq 0.6479$.

The analysis up to this point is incomplete in that V_m remains unknown. This quantity is determined by the higher-order terms of the asymptotic expansions, whose features will be only summarized here. The second term of the outer expansion (17), which is forced by the displacement $\mathscr{A}(\pi V_m/H_0)^{\frac{1}{2}}$ of the viscous sublayer, obeys a linear system of equations whose solution can be written in closed form, but does not determine V_m. The next term (U_2, V_2, A_2) does not determine V_m either. The resulting linear equations at this order, as well as those for U_1 and V_1, have singular regular points at $Y = 0$ and $Y = H_0$ and the expansion of U_2 near the upper singular point contains the logarithmic term

$$\pi^2\left[\frac{\pi^2}{2H_0} - \mathscr{A}\left(\frac{\pi V_m}{H_0}\right)^{\frac{1}{2}}\right]\left(1 - \frac{Y}{H_0}\right)^2 \ln\left(1 - \frac{Y}{H_0}\right), \tag{22}$$

which induces a term proportional to $\ln(1-Y/H_0)$ in U_4 (the coefficient of

$$(X_t-X)[-\ln(X_t-X)]^{-2}$$

in (17)). Since this is not admissible (the boundary conditions (4) give $U_i'(H_0) = V_i(H_0) = 0$ for all the logarithmic terms in (17)), nor can it apparently be fixed by introducing another viscous region near the surface to satisfy the boundary conditions there, (22) must be zero, i.e. $V_m H_0 = \pi^3/4\mathscr{A}^2 \simeq 18.4660$, which completes the solution near the rear tip of the bubble. Note that the second term in square brackets in (22), proportional to $\mathscr{A}$, is due to the displacement of the viscous sublayer, while the other term comes entirely from the derivatives of the logarithms in the outer expansion (17). The fact that both terms appear in U_2, cancelling each other, is a consequence of the choice $k = 2$ (cf. the discussion above (17)), which is thereby justified.

The neat flux of the layer, equal to $S_l^{\frac{1}{2}}$ in the present variables, has been neglected in the analysis of the bubble. This flux will be felt in a shorter region of streamwise length ΔX, with $\Delta X(\ln \Delta X)^2 = S_l^{\frac{1}{2}}$, centred about $X = X_t$, and comprising: a viscous sublayer of thickness $(-\ln \Delta X)^{-1}$, and inviscid vortical flow (whose vorticity depends linearly on the stream function), and a region of relatively stagnant fluid at the upper right, which tends to cover half of the layer far downstream. Further downstream, the growth of the viscous sublayer and of the shear layer above the inviscid flow eventually leads to the parabolic velocity profile mentioned in §2.

A couple of remarks follow, to close this section. First, an analysis similar to the previous one can be carried out for a circular jump, taking into account the divergence of the flow in its interior. For large values of the Froude number at the inlet of the jump ($S_l \ll 1$), such an analysis gives (h_2/h_1) and (r_2/r_1) of order $S_l^{-(n_r+2)/3(n_r+1)}$ with $n_r = (19)^{\frac{1}{2}}-4$. Here r_1 and r_2 are the radii of the fore and aft ends of the jump, and h_1 and h_2 are the corresponding depths. These results, however, are of more limited applicability than those for the planar case, because very small values of S_l are not so easily attained over an extended region owing to the rapid decay of the local Froude number in the axisymmetric case (S_l is proportional to r_1^8 for the axisymmetric Watson solution).

Secondly, though no attempt to analyse the stability of the asymptotic solution is made here, Bickley's jet profile at the upper part of the jump should be expected to become unstable if S_l becomes too small keeping $Re = Q/\nu$ constant. This is because the Reynolds number of the flow at the inlet of the jump does not depend on x_J, being equal to Re for the planar configuration at hand, while the size of the jump relative to x_J, and therefore the Reynolds number of the jet, $O(Re\,\tilde{x}^{\frac{1}{3}})$, and the length available for any instability to develop, increases with decreasing S_l.

This instability, if it exists, would not be unlike that found by Craik *et al.* (1981) for circular jumps, though their interpretation is different, and associated to the disappearance of the recirculation bubble. They find that, keeping the flux constant, the flow becomes oscillatory and then turbulent in the rear part of the jump when the downstream depth is increased and the jump is thereby pushed upstream into regions of higher Froude number. Contrarily to the case of planar flow, the length of the jump is seen to decrease in this process, but the Reynolds number of the axisymmetric flow increases (being proportional to the inverse of the standoff distance of the jump), which most probably offsets the decrease of length and may lead to the same instability as conjectured before. Experiments on circular jumps showing a wider range of flow and stability conditions have been carried out by Liu & Lienhard (1993); these authors suggest that some of the observed phenomena might be specific to the axisymmetric configuration and related to the effect of surface tension.

5. Effects of surface tension and streamline curvature

The effects of the surface tension and the cross-stream pressure variation induced by streamline curvature in the interaction region at the leading end of the jump were studied by Bowles & Smith (1992). Here, the influence of these effects on the rest of the jump and on the flow approaching the edge of the plate is discussed.

In the non-dimensional variables of §2, the pressure jump across the slightly curved surface of the liquid due to the surface tension is

$$\Delta p_T = -T\frac{\mathrm{d}^2 h}{\mathrm{d}x^2}, \quad \text{where} \quad T = \frac{\sigma \nu^3 \bar{l}}{\rho Q^5}. \tag{23}$$

The cross-stream pressure variation due to the curvature of the streamlines is

$$\Delta p_c = Re^{-2}\frac{\mathrm{d}^2 h}{\mathrm{d}x^2}F(y), \tag{24}$$

where

$$F(y) = \int_y^h u^2\,\mathrm{d}y' - S\int_y^h u^2\left[\int_{y'}^h \frac{\mathrm{d}y''}{u^2}\right]\mathrm{d}y'. \tag{25}$$

The first term of $F(y)$ is a standard result (see, e.g. Messiter & Liñán 1976; Smith & Duck 1977). The second term is much smaller than the first one, of $O(S^{\frac{1}{2}})$ in the interaction region at the leading tip of a strong jump, where $u = O(S^{\frac{1}{2}})$ and $h = O(S^{-\frac{1}{2}})$, but becomes important near the edge of the plate, where a strong streamwise pressure gradient exists, and it is necessary to make (25) uniformly valid. A derivation of (24) is given in the second part of the Appendix.

To take into account the pressure variations (23) and (24), the numerical method of §2 was slightly modified, writing the momentum equation in the form

$$\frac{\partial u}{\partial t} + u\frac{\partial u}{\partial x} + v\frac{\partial u}{\partial y} = -S\frac{\partial h}{\partial x} - \frac{\partial}{\partial x}\{[T - Re^{-2}F(y)]\tilde{\Pi}\} + \frac{\partial^2 u}{\partial y^2}, \tag{26}$$

where t is a pseudo-time and $\tilde{\Pi}$ satisfies $A\,\partial h/\partial t = \partial^2 h/\partial x^2 + \tilde{\Pi}$. This amounts to assigning a fictitious inertia to the surface, measured by the constant A, which facilitates the numerical convergence without affecting the final steady result.

The conditions for the pressure variations (23) and (24) to influence the viscous sublayer of the interaction region are $TS^3 = O(1)$ and $Re/S^{\frac{7}{4}} = O(1)$, respectively, as can be verified by using the estimate $\Delta x = O(S^{-2}) \ll 1$ for the length of this region. On the other hand, the condition $Re\,T^{\frac{1}{2}}/S^{\frac{1}{8}} \ll 1$ is obtained in the Appendix for a steady solution to exist near the edge of the plate (cf. the discussion following (A 15)). This condition is incompatible with the previous ones, which means that the surface tension cannot be strong enough for its effect to appear in the interaction region unless the plate is slightly rounded, being convex toward the fluid. The numerical results of this section were obtained for a plate that is flat and horizontal down to a certain distance to the edge, in the range $T^{\frac{1}{2}}/S^{\frac{1}{2}} \ll (1-x) \ll T^{(\sigma+2)/5}/S^{(\sigma+2)/15}$ (with $\sigma \simeq 0.3640$), and then curves downward. According to the results of the Appendix, the relations (A 15) should hold in this range of $(1-x)$, and the second derivative of the second of these relations implies

$$\frac{\mathrm{d}^2 h}{\mathrm{d}x^2} = \frac{1+2\sigma}{1-2\sigma}\frac{\mathrm{d}h/\mathrm{d}x}{1-x}, \tag{27}$$

which makes a suitable boundary condition for the equations (1) and (26). Proceeding in this manner, the results depend only on the value of $(1-x)$ at which (27) is imposed,

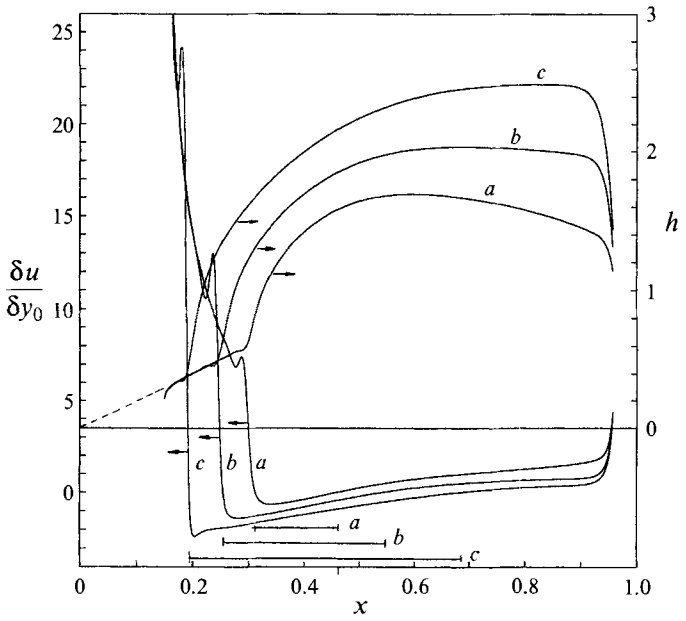

FIGURE 7. Skin friction and liquid depth for $S = 1.04$, $Re^{-1} = 0$, and three values of T. a, 4.705×10^{-5}; b, 1.412×10^{-4}; c, 2.353×10^{-4}. The lengths of the recirculation bubbles are indicated in the lower part of the figure. The inlet conditions are (5) with $h_I = 0.2125$.

which was fixed once and for all to study the influence of the parameters T and Re^{-1} on the position and structure of the jump.

Figure 7 shows the skin friction and liquid depth for $S = 1.04$, $Re^{-1} = 0$, and three different values of T. The rapid rise of the surface near the inlet is due to the viscous adjustment of the flow, because the inlet condition (5) was used, with $h_I = 0.2125$. One effect of the surface tension is to make the surface oscillate ahead of its main elevation, a result predicted by the interactive theory of Bowles & Smith and observed in the experiments of Craik *et al.*, among others. A single small rise and dip of the surface can be seen in figure 7, to be compared with figure 6 of Craik *et al.* (1981), and an associated inverse oscillation appears in the skin friction. Two other effects of capillarity, associated with the curvature of the surface near the edge of the plate, are to increase the size of the recirculation bubble and to reduce the (negative) slope of the surface downstream of the jump. Both of these effects become more pronounced when T is increased or when the boundary condition (27) is imposed at a smaller value of $(1-x)$, until finally the numerical method fails to converge. Results for larger values of S, or with the inlet condition (11) instead of (5), show the same trend, but with jumps shorter than those of figure 7.

The interaction problem with the pressure–displacement relation (24) is known to have a characteristic singularity (Smith 1977) representing a strong convergence of the flow toward the wall, with the pressure decreasing as $-(x_s - x)^{-4}$ near the position (x_s) of the singularity. Although this singularity could conceivably be avoided for the problem at hand (Bowles & Smith 1992), it seems that the numerical method easily brings it in when Re^{-2}/T grows, both at what would be the interaction region and near the edge of the plate. The influence of Re^{-1} on the numerical solution is at first opposite to that of T, as expected; most noticeably, the bubble becomes slightly shorter as Re^{-1} increases. Then, at a certain value of this parameter depending on S and T, the solution undergoes an abrupt change, with a roller appearing at the surface and the

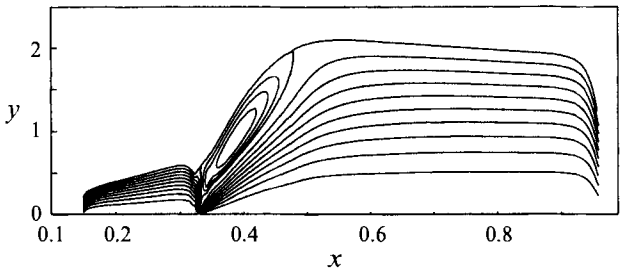

FIGURE 8. Streamlines of the flow for $S = 1.04$, $T = 1.412 \times 10^{-4}$ and $Re^{-1} = 1.2 \times 10^{-4}$. The inlet conditions are (5) with $h_I = 0.2125$.

fluid flowing underneath (see figure 8). Locally, this solution resembles the singularity predicted by Smith (1977), and the numerical results are probably meaningless in the region of strong convergence. Interestingly, the numerical computation does not fail completely when Re^{-1} is increased above the value leading to the first appearance of the roller, which possibly has to do with the fact that the singularity is never completely realized in the present flow, because its existence depends on a continuous decrease of the depth leading to a continuous decrease of the pressure, whereas such a decrease of depth is arrested here by the recirculating fluid in the roller falling onto the incoming flow. It was kindly pointed out by a referee that the boundary-layer approximation need not fail locally under these conditions. While this issue remains undecided, further computations with refined grids, aimed at fully resolving the structure of the boundary layer, suggest that the region of influence of the roller's tip shrinks when the pitch of the grid is decreased, and its effect seems too weak to bring the solution out of the singularity. Note also that a steady roller with a hydrostatic or quasi-hydrostatic pressure distribution can only exist if its size is sufficiently large to have regions of positive and negative shear stress at its bottom surface, which must balance each other, because the net horizontal pressure force acting on the bubble is zero or negligible.

Obviously, solutions like the one in figure 8 cannot be accepted without reservation, but, on the other hand, the flow depicted in this figure has the correct general appearance of many hydraulic jumps, so that the numerical solution might still be capturing part of the reality. If these results are accepted as a qualitative guide, an asymptotic structure can be constructed for this kind of jump in the limit $S \to \infty$. An order-of-magnitude analysis, proceeding along the lines of §4, leads to values of the length of the jump and the depth of the liquid at its downstream side of orders $\Delta\tilde{x} = O(S_l^{-\frac{4}{7}})$ and $\tilde{h}_2 = O(S_l^{-\frac{3}{7}})$ (the tilde variables and S_l are defined in the first paragraph of §4), while the main features of the asymptotic structure are as follow: the high-Froude-number flow crossing under the toe of the jump forms a wall jet whose thickness and mass flux are proportional to $\tilde{x}^{\frac{3}{4}}$ and $\tilde{x}^{\frac{1}{4}}$, respectively (Glauert 1956). Since this jet ingests fluid from the overhead roller, where the Bernoulli constant is uniform, $O(S_l \tilde{h}_2)$, the depth of the roller must be of order $\tilde{x}^{\frac{1}{4}}/(S_l \tilde{h}^2)$ in its fore part, until the velocities of the fluid in the jet and in the roller become finally comparable for $\tilde{x} = O(S_l^{-\frac{4}{7}})$, which corresponds to the bulk of the roller. The flow separates from the plate in the rear part of the jump, leading to a secondary recirculation bubble already hinted at by the strong divergence of the streamlines in figure 8 and actually realized in other computations. The terminal structure of the secondary bubble is like the one described in §4.

I am grateful to Professors A. Liñán and J. M. Vega for many enlightening discussions. This work was partially supported by the Spanish DGICYT under grants ESP 187/90 and PB92-1075.

Appendix. Structure of the liquid layer near the edge of the plate

In this Appendix the subcritical boundary-layer flow approaching the edge of the plate is analysed. A boundary condition for equations (1) and (2), reflecting the singularity that the boundary-layer solution develops at the edge, will emerge from this analysis.

When $S \gg 1$, the flow downstream of the jump is determined by the balance of pressure and viscous forces over most of the plate, which yields a parabolic velocity profile and $h = [12(1-x)/S]^{\frac{1}{3}}$ (see §2). Evaluating the convective terms of the momentum equation (2) with this approximate solution, they can be seen to become comparable to the other terms in the equation for $(1-x) = O(S^{-\frac{1}{3}}) \ll 1$. Thus the effect of the inertia of the fluid reappears at this short distance from the edge, where $(y, h) = O(S^{-\frac{1}{3}})$, $(u, v) = O(S^{\frac{1}{3}})$, and

$$[x_e, y_e, h_e, u_e, v_e, S_e] = [S^{\frac{1}{3}}(x-1), S^{\frac{1}{3}}y, S^{\frac{1}{3}}h, u/S^{\frac{1}{3}}, v/S^{\frac{1}{3}}, 1]$$

are of order unity. These scaled variables will be used in what follows, but S_e, which is equal to one, will be left in the equations, partly to help with the bookkeeping, and partly because the previous transformation is not required when $S = O(1)$, in which case the subscript e can be deleted and $S_e = S$.

Matching of the solution of (1)–(4) in the region $x_e = O(1)$ with the turn around region mentioned in §2 requires that the hydrostatic pressure gradient and the wall shear stress in the boundary-layer solution both tend to infinity at the edge. Under the action of this strong acceleration, viscous effects are confined to a thin sublayer near the plate, while the solution in the rest of the layer is of the form

$$u_e = u^*(y_e) + (-x_e)^{\delta} U(y_e), \quad v_e = (-x_e)^{\delta-1} V(y_e), \quad h_e = h^* + (-x_e)^{\delta} H, \quad \text{(A 1)}$$

for some $0 < \delta < 1$. Here h^* and $u^*(y_e)$ are the unknown limiting depth and velocity distribution, with $u^* \simeq \gamma y_e^{\sigma}$, for some $\sigma < 1$, when $y_e \ll 1$. The equations (1)–(4), linearized about the limiting velocity yield

$$V = -\delta H u^* \left[1 - S_e \int_{y_e}^{h^*} \frac{\mathrm{d}y_e}{u^{*2}}\right], \quad \text{(A 2)}$$

and $U = V'/\delta$, which is of the form

$$U \simeq \left(S_e \int_0^{h^*} \frac{\mathrm{d}y_e}{u^{*2}} - 1\right) \frac{\gamma\sigma H}{y_e^{1-\sigma}} - \frac{1-\sigma}{1-2\sigma} \frac{S_e H}{\gamma y_e^{\sigma}} + \ldots \quad \text{for } y_e \ll 1. \quad \text{(A 3)}$$

The flow in the viscous sublayer is affected by the pressure force due to the gradient of h_e in (A 1). The thickness of this sublayer, y_v say, and a first relation between the two unknown parameters σ and δ can be obtained from the balance of convection, pressure gradient, and viscous forces in the sublayer: $u_e^2/(-x_e) \sim S_l(h_e - h^*)/(-x_e) \sim u_e/y_v^2$, with $u_e = O(y_v^{\sigma})$ to match $u^*(y_e)$ in (A 1), and $(h_e - h^*) = O[(-x_e)^{\delta}]$. This gives $y_v = O[(-x_e)^{1/(\sigma+2)}]$ and $\delta = 2\sigma/(\sigma+2)$. The solution in the viscous sublayer is of the form (in terms of the stream function)

$$\psi = (-x_e)^{(\sigma+1)/(\sigma+2)} g(\eta), \quad \text{with} \quad \eta = \frac{y_e}{(-x_e)^{1/(\sigma+2)}}, \quad \text{(A 4)}$$

where $g(\eta)$ satisfies $(\sigma+2)g''' + \sigma g'^2 + (\sigma+1)gg'' + 2\sigma S_e H = 0$ (obtained by carrying (A 4) into (2)), with the boundary conditions $g(0) = g'(0) = 0$ and the matching

condition $g' \sim \gamma\eta^\sigma$ for $\eta \to \infty$. The solution of this problem has been analysed elsewhere (Higuera & Liñán 1993; Higuera 1993), and matching to the outer solution (A 1)–(A 3) terms out to require that the coefficient of $1/y_e^{1-\sigma}$ in (A 3) be zero and that $\sigma = \sigma_c \simeq 0.364$ (hence $\delta \simeq 0.308$). The first of these conditions means that the speed of the upstream propagating waves becomes zero at the edge.

Let us consider now the effect of the surface tension on the flow near the edge. In the variables introduced before, the pressure variation (23) due to the surface tension becomes $-T_e \mathrm{d}^2 h_e/\mathrm{d}x_e^2$, where $T_e = T/S^{\frac{1}{3}}$ will be assumed to be small. Including this term in the momentum equation, the solution of (1), (3)–(5) and (26) in the inviscid region near the edge of the plate is of the form

$$u_e = u^*(y_e) + U_e(x_e, y_e), \quad v_e = V_e(x_e, y_e), \quad h_e = h^* + H_e(x_e), \quad \text{with} \quad (U_e, H_e) \ll 1, \tag{A 5}$$

where (using primes to denote y_e-derivatives of u^* and x_e-derivatives of H_e),

$$\frac{\partial U_e}{\partial x_e} + \frac{\partial V_e}{\partial y_e} = 0, \tag{A 6}$$

$$u^* \frac{\partial U_e}{\partial x_e} + u^{*\prime} V_e = -S_e H_e' + T_e H_e''', \tag{A 7}$$

$$V_e = 0 \quad \text{at} \quad y_e = 0, \tag{A 8}$$

$$V_e = u^* H_e' \quad \text{at} \quad y_e = h^*, \tag{A 9}$$

whose solution is

$$V_e = u^* H_e' - (S_e H_e' - T_e H_e''') u^* \int_{y_e}^{h^*} \frac{\mathrm{d}y_e}{u^{*2}}, \tag{A 10}$$

and a similar expression for U_e. Near the wall (where $u^* \simeq \gamma y_e^\sigma$) this U_e takes the form

$$U_e = -\frac{\gamma\sigma T_e H_e''}{S_e y_e^{1-\sigma}} - \frac{1-\sigma}{1-2\sigma} \frac{(S_e H_e - T_e H_e'')}{\gamma y_e^\sigma} + \ldots, \tag{A 11}$$

where use has been made of the criticality condition $S_e \int_0^{h^*} (\mathrm{d}y_e/u^{*2}) = 1$ satisfied by the limiting velocity.

As before, the condition that the hydrostatic pressure gradient should drive the flow in the nonlinear viscous sublayer (where $y_e = O[(-x_e)^{1/(\sigma+2)}]$) gives $H_e = O[(-x_e)^{2\sigma/(\sigma+2)}]$. In addition, the first term of (A 11) is also of the order of u^* in the sublayer when $(-x_e) = O(T_e^{(\sigma+2)/5})$. Using then the scaled variables $x_1 = x_e/T_e^{(\sigma+2)/5}$, $y_1 = y_e/T_e^{1/5}$, $H_1 = H_e/T_e^{2\sigma/5}$, and the streamfunction ψ_1 scaled with $T_e^{(\sigma+1)/5}$, the problem in the viscous sublayer becomes

$$\frac{\partial \psi_1}{\partial y_1} \frac{\partial^2 \psi_1}{\partial x_1 \partial y_1} - \frac{\partial \psi_1}{\partial x_1} \frac{\partial^2 \psi_1}{\partial y_1^2} = -S_e H_1' + \frac{\partial^3 \psi_1}{\partial y_1^3}, \tag{A 12}$$

$$\psi_1 = \frac{\partial \psi_1}{\partial y_1} = 0 \quad \text{at} \quad y_1 = 0, \tag{A 13}$$

$$\frac{\partial \psi_1}{\partial y_1} \to \gamma y_1^\sigma - \frac{\gamma\sigma H_1''}{S_e y_1^{1-\sigma}} - \frac{1-\sigma}{1-2\sigma} \frac{S_e H_1}{\gamma y_1^\sigma} \quad \text{for} \quad y_1 \to \infty. \tag{A 14}$$

Note that the velocity perturbations induced by the surface tension in the inviscid region of the flow (proportional to T_e) are small compared with the values of U_e and V_e in the absence of surface tension, but these perturbations diverge at the plate faster

than the unperturbed quantities and become comparable to them in the viscous sublayer. The pressure perturbation due to the surface tension is also much smaller than the hydrostatic pressure and does not affect directly the flow in the viscous sublayer.

The problem (A 12)–(A 14) has a solution with the second term of (A 14) going to zero for $x_1 \to -\infty$, which coincides with the solution (A 4) for $T_e = 0$ (with x_e replaced by x_1 and $\eta = y_1/(-x_1)^{1/(\sigma+2)}$). Then, under the effect of the second term of (A 14), the solution of (A 12)–(A 14) develops a singularity at a finite value of x_1, which can be taken as $x_1 = 0$ after an appropriate shift. For $|x_1| \ll 1$, the viscous effects are confined to a thin sub-sublayer, whereas the thickness of the region of nonlinear response and the value of H_1 are

$$y_1 = O(|x_1|^{-2/(1-2\sigma)}), \quad H_1 = O(|x_1|^{-4\sigma/(1-2\sigma)}). \tag{A 15}$$

These results come from the balance of inertia and pressure forces in (A 12) and of the three terms of (A 14). The region of nonlinear response will cover the whole liquid layer when $|x_1| = O(T_e^{(1-2\sigma)/10})$, or $|x_e| = O(T_e^{\frac{1}{2}})$, which is the order of the smallest $|x_e|$ for which a solution of the boundary-layer equations exists. The pressure perturbation due to the surface tension influences the whole layer for these values of $|x_e|$, and would become larger than the dynamical pressure of the flow of $|x_e| \ll O(T_e^{\frac{1}{2}})$, thus preventing any outward motion. Hence $T_e^{\frac{1}{2}}$ is the order of the minimum allowable curvature radius of the solid surface in the region around the edges for which a steady solution exists. The flow for smaller curvature radii will probably be time periodic, with liquid dammed most of the time under a meniscus at the edge, and released only when its volume reaches a certain critical value (see, e.g. Gañán 1989 for the conditions of existence of an anchored meniscus). A stationary solution may also exist for a sharp-edged plate if $Re\, T_e^{\frac{1}{2}} \ll 1$ (or $Re\, T^{\frac{1}{2}}/S^{\frac{1}{6}} \ll 1$ in the original variables of §2), because then the flow would enter the turn-around region before the surface tension overpressure becomes too large.

The effect of the cross-stream pressure variation Δp_c due to the curvature of the stream-lines can be analysed in a similar way. Writing again the solution in the inviscid region near the edge in the form (A 5), the equations describing the motion in this region are

$$\frac{\partial U_e}{\partial x_e} + \frac{\partial V_e}{\partial y_e} = 0, \tag{A 16}$$

$$u^* \frac{\partial U_e}{\partial x_e} + u^{*\prime} V_e = -S_e H_e' - \frac{\partial \Delta p_c}{\partial x_e}, \tag{A 17}$$

$$Re^{-2} u^* \frac{\partial V_e}{\partial x_e} = -\frac{\partial \Delta p_c}{\partial y_e}, \tag{A 18}$$

$$V_e = 0 \quad \text{at} \quad y_e = 0, \tag{A 19}$$

$$V_e = u^* H_e', \quad \Delta p_c = 0 \quad \text{at} \quad y_e = h^*, \tag{A 20}$$

where (A 18) is the vertical component of the momentum equation. Advancing that, as for the case of the surface tension, $\Delta p_c \ll S_e H_e$ and that the velocity perturbations due to Δp_c are small compared with the values of U_e and V_e with $Re^{-1} = 0$, the unperturbed V_e (given by (A 10) with $T_e = 0$) can be used in the left-hand side of (A 18), leading to

$$\Delta p_c = Re^{-2} H_e'' F(y_e), \quad \text{with} \quad F(y_e) = \int_{y_e}^{h^*} u^{*2} \left[1 - S_e \int_{y_e'}^{h^*} \frac{\mathrm{d}y_e''}{u^{*2}} \right] \mathrm{d}y_e'. \tag{A 21}$$

Then (A 16) and (A 17) with the conditions (A 19) and (A 20) determine U_e and V_e, and the expansion of this solution for $y_e \ll 1$ is, neglecting small terms,

$$U_e = Re^{-2}\left(\int_0^{h^*} \frac{F\,dy_e}{u^{*2}}\right)\frac{\gamma\sigma H_e''}{y_e^{1-\sigma}} - \frac{1-\sigma}{1-2\sigma}\frac{S_e H_e}{\gamma y_e^{\sigma}} + \ldots . \tag{A 22}$$

This is analogous to (A 11), with $Re^{-2}\int_0^{h^*}(F/u^{*2})\,dy_e$ playing the role of $-T_e/S_e$, and the results of the previous case relative to the viscous sublayer apply also here. In particular, the condition $|x_e| \ll T_e^{\frac{1}{3}}$ for the boundary-layer equations to have a solution becomes now $|x_e| \ll Re^{-1}$, which is obviously satisfied, for $|x_e| = O(Re^{-1})$ corresponds to the turn-around region.

REFERENCES

BATCHELOR, G. K. 1970 *An Introduction to Fluid Dynamics*, pp. 344–345. Cambridge University Press.

BOHR, T., DIMON, P. & PUTKARADZE, V. 1993 Shallow-water approach to the circular hydraulic jump. *J. Fluid Mech.* **254**, 635–648.

BOUHADEF, M. 1978 Etalement en couche mince d'un jet liquide cylindrique vertical sur un plan horizontal. *Z. angew. Math. Phys.* **29**, 157–167.

BOWLES, R. I. 1990 Applications of nonlinear viscous–inviscid interactions in liquid layer flows and transonic boundary layer transition. PhD thesis, University of London.

BOWLES, R. I. & SMITH, F. T. 1992 The standing hydraulic jump: theory, computations and comparisons with experiments. *J. Fluid Mech.* **242**, 145–168.

BROWN, S. N., STEWARTSON, K. & WILLIAMS, P. G. 1975 On expansive free interactions in boundary layers. *Proc. R. Soc. Edinburgh* **74A**, 21.

CHAUDHURY, Z. H. 1964 Heat transfer in a radial liquid jet. *J. Fluid Mech.* **20**, 501–511.

CRAIK, A. D. D., LATHAM, R. C., FAWKES, M. J. & GRIBBON, P. W. F. 1981 The circular hydraulic jump. *J. Fluid Mech.* **112**, 347–362.

DANIELS, P. G. 1992 A singularity in thermal boundary layer flow on a horizontal surface. *J. Fluid Mech.* **242**, 419–440.

GAJJAR, J. S. B. & SMITH, F. T. 1983 On hypersonic self-induced separation, hydraulic jumps and boundary layers with algebraic growth. *Mathematika* **30**, 77–91.

GAÑÁN, A. M. 1989 Análisis nodal de zonas líquidas axilsimétricas confinadas por tensión superficial. PhD thesis, University of Sevilla, Spain.

GLAUERT, M. B. 1956 The wall jet. *J. Fluid Mech.* **1**, 625–643.

HIGUERA, F. J. 1993 Natural convection below a downward facing horizontal plate. *Eur. J. Mech.* B **12**, 289–311.

HIGUERA, F. J. & LIÑÁN, A. 1993 Choking conditions for nonuniform viscous flows. *Phys. Fluids* A **5**, 768–770.

ISHIGAI, S., NAKANISHI, S., MIZUNO, M. & IMAMURA, T. 1977 Heat transfer of the impinging round water jet in the interference zone of film flow along the wall. *Bull. JSME* **20**, 85–92.

KURIHARA, M. 1946 Laminar flow in a horizontal liquid layer. *Rep. of the Res. Inst. for Fluid Engng Kyusyu Imp. Univ.* **3-1946**, 11.

LARRAS, M. J. 1962 Ressaut circulaire sur fond parfaitement lisse. *CR Acad. Sci. Paris* **225**, 837–839.

LIU, X. & LIENHARD, V. 1993 The hydraulic jump in circular jet impingement and in other thin liquid films. *Exps Fluids* **15**, 108–116.

MESSITER, A. F. & LIÑÁN, A. 1976 The vertical plate in laminar free convection: effects of leading and trailing edges and discontinuous temperature. *Z. angew. Math. Phys.* **27**, 632–651.

NAKORYAKOV, V. E., POKUSAEV, B. G. & TROYAN, E. N. 1978 Impingement of an axisymmetric liquid jet on a barrier. *Intl J. Heat Mass Transfer* **21**, 1175–1184.

OLSSON, R. G. & TURKDOGAN, E. T. 1966 Radial spread of a liquid stream on a horizontal plate. *Nature* **211**, 813–816.

RAHMAN, M. M., HANKEY, W. L. & FAGHRI, A. 1991 Analysis of the fluid flow and heat transfer in a thin liquid film in the presence and absence of gravity. *Intl J. Heat Mass Transfer* **34**, 103–114.

SMITH, F. T. 1977 Upstream interaction in channel flow. *J. Fluid Mech.* **79**, 631–655.

SMITH, F. T. & BROTHERTON-RATCLIFFE, R. V. 1990 *Theoret. Comput. Fluid Dyn.* **1**, 21.

SMITH, F. T. & DUCK, P. W. 1977 Separation of jets and thermal boundary layers from a wall. *Q. J. Mech. Appl. Maths* **30**, 143–156.

TANI, I. 1948 Flow separation in thin liquid layers. *J. Phys. Soc. Japan* **4**, 212–215.

WATSON, E. J. 1964 The radial spread of a liquid jet over a horizontal plate. *J. Fluid Mech.* **20**, 481–499.